Chinese Chemical Letters 35 (2024) 108689

Contents lists available at ScienceDirect

Chinese Chemical Letters

journal homepage: www.elsevier.com/locate/cclet

Bi-doped carbon quantum dots functionalized liposomes with fluorescence visualization imaging for tumor diagnosis and treatment

Peide Zhu[a,1], Yangjia Liu[b,1], Yaoyao Tang[a,1], Siqi Zhu[c], Xinyang Liu[a], Lei Yin[c], Quan Liu[c], Zhiqiang Yu[b], Quan Xu[a,*], Dixian Luo[c,*], Juncheng Wang[d,*]

[a] State Key Laboratory of Heavy Oil Processing, China University of Petroleum-Beijing, Beijing 102249, China
[b] Department of Laboratory Medicine, Dongguan Institute of Clinical Cancer Research, Affiliated Dongguan Hospital, Southern Medical University, Dongguan 523058, China
[c] Department of Laboratory Medicine, Huazhong University of Science and Technology Union Shenzhen Hospital (Nanshan Hospital), Shenzhen 518052, China
[d] Institute of Stomatology, First Medical Center, Chinese PLA General Hospital, Beijing 100853, China

ARTICLE INFO

Article history:
Received 10 April 2023
Revised 9 June 2023
Accepted 12 June 2023
Available online 15 June 2023

Keywords:
Bi-doped CQDs
Lipo/Bi-doped CQDs
pH sensitivity
In vitro/*in vivo* imaging
Diagnosis and treatment integration

ABSTRACT

Liposomes are one of the significant classes of antitumor nanomaterials and the most successful nanomedicine drugs in clinical translation. However, it is difficult to accurately reveal liposome delivery modes and drug release rates at different pH values to assess the biodistribution and drug delivery pathways *in vivo*. Here, we established a strategy to integrate Bi-doped carbon quantum dots (CQDs) with liposomes to produce fluorescence visualization and therapeutic effects, namely lipo/Bi-doped CQDs. Lipo/Bi-doped CQDs show good water solubility and physicochemical properties, which can be used for *in vitro* labeling of colon cancer (CT26) cells and *in vivo* imaging localization tracking tumors for monitoring. Simultaneously, thanks to the excellent pH sensitivity and ion doping characteristic of Bi-doped CQDs, lipo/Bi-doped CQDs can be used to reveal the drug release rate of liposomes at different pH values and exhibit potential effects *in vivo* antitumor therapy.

Advances in biotechnology and medicine have promoted the use of novel nanoparticles in diagnostic therapy, which are significant in clinically relevant cancer models because of their higher loading capacity, the controllable concentration of chemotherapeutic agents, easy surface functionalization, and excellent photostability compared to conventional molecular-level compounds [1–4]. In recent years, researchers have focused on exploring novel nanoparticles that can integrate diagnostic and therapeutic and have developed various nanomaterials such as gold nanoshells [5,6], carbon quantum dots (CQDs) [7], carbon nanotubes [8,9], and semiconductor quantum dots (SQDs) [10]. CQDs are a new zero-dimensional carbon nanomaterial of great interest in carbon nanostructures consisting of multifunctional targeting, diagnostic and therapeutic modalities due to their unique properties [4,7,10]. For example, with radioisotope integrated CQDs can be used for dual-mode imaging, and CQDs bound to drugs or peptides can be used as diagnostic and therapeutic nanomaterials [4,11,12]. Although CQDs have been used to some extent in synergy with other materials for the diagnostic treatment of tumors, Bi-doped CQDs as diagnostic and therapeutic agents have not been reported so far.

Liposomes, a bilayer membrane structure composed of phospholipids and cholesterol molecules, have attracted much attention recently for their ability to control drug release and cancer diagnosis [2,13]. Moreover, as a drug nanocarrier system, it is necessary to evaluate its drug delivery and monitor its uptake and distribution in cells, tissues, and organs [14]. However, most of the reported methods to generate fluorescent liposomes by loading fluorescent materials, such as aggregation-induced luminescence (AIE) dyes or SQDs have various drawbacks, such as single performance, complicated co-loading procedures, and quenching caused by fluorescence aggregation [15,16]. In contrast, CQDs have great potential for monitoring drug release, uptake, and distribution in cellular tissues [2,17-19]. For example, Feng *et al.* developed a tumor cell microenvironment-responsive drug nanocarrier based on switchable carbon dots (CDs) loaded with cisplatin(IV) prodrugs (CDs-Pt(IV)@PEG-(PAH/DMMA)). In the tumor microenvironment, converting the dimethylmaleic acid anionic polymer on the carrier surface to a cationic polymer resulted in solid electrostatic repulsion and drug release of CDs-Pt(IV), resulting in improved tumor

* Corresponding authors.
E-mail addresses: xuquan@cup.edu.cn (Q. Xu), luodixian_2@163.com (D. Luo), wbhwjc527@126.com (J. Wang).
[1] These authors contributed equally to this work.

https://doi.org/10.1016/j.cclet.2023.108689
1001-8417/

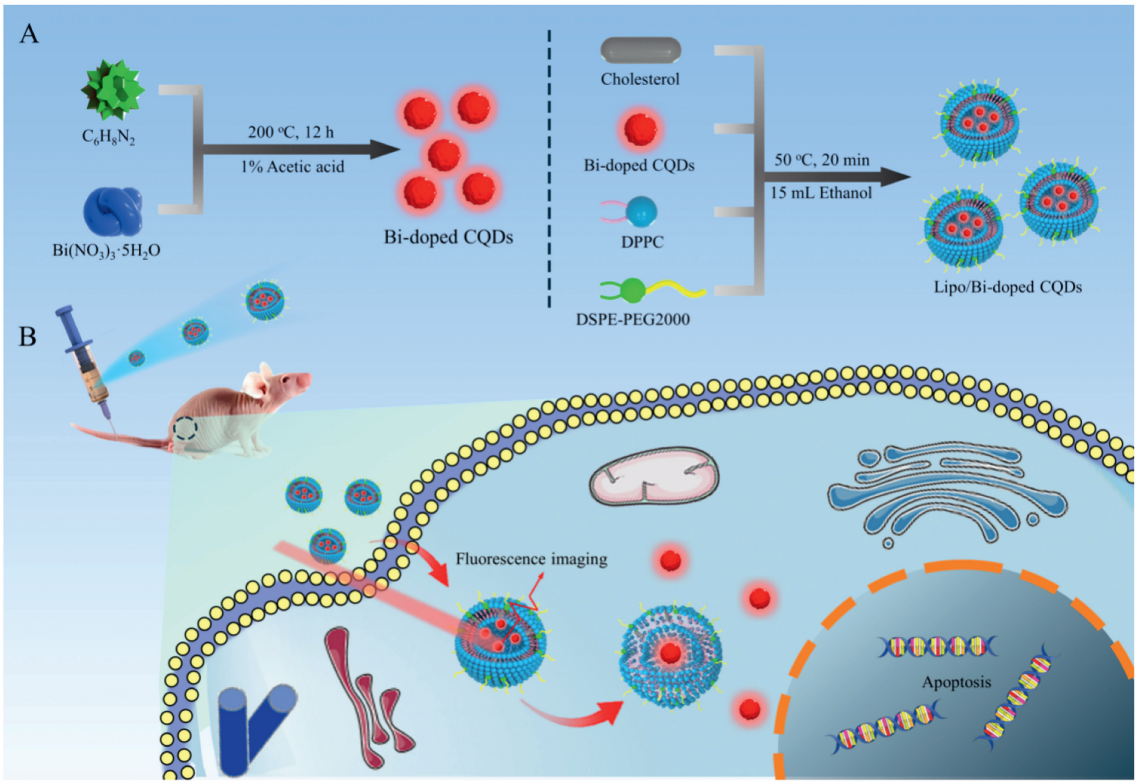

Scheme 1. Schematic preparation process of Bi-doped CQDs and lipo/Bi-doped CQDs and their application in diagnosis and therapy.

suppression and reduced toxic effects [17]. Gong *et al.* prepared a simple and sensitive two-photon imaging of fluorescent N-doped CDs to intuitively monitor the loading, endocytosis, cell distribution, and release process of doxorubicin-based on the fluorescence resonance energy transfer (FRET) effect, showing great potential for applications in biomedical and bioimaging fields [19]. However, to our knowledge, studies using Bi-doped CQDs to reveal the drug release rate of liposomes at different pH values and as a diagnostic and therapeutic agent have yet to be reported previously.

The limitations of functional liposomes and the unique properties of CQDs inspire us. In this study, we first developed Bi-doped CQDs with diagnostic and therapeutic potential and further combined them with liposomes to form Bi-doped CQDs functionalized liposomes (lipo/Bi-doped CQDs). Lipo/Bi-doped CQDs are expected to produce bright red fluorescence while avoiding the elimination of Bi-doped CQDs before reaching the tumor region due to their increased particle size and specific targeting. In addition, Bi-doped CQDs also provide liposomes with multiple functions: (1) monitoring the degradation rate of liposomes at different pH values; (2) performance of drug delivery and imaging; and (3) enhanced anticancer effect. In conclusion, our results suggest that bright red fluorescence and efficient colon cancer treatment make lipo/Bi-doped CQDs a versatile drug delivery system guided by an imaging track.

As shown in Scheme 1A, the Bi-doped CQDs were prepared by solvothermal polymerization of bismuth nitrate and *o*-phenylenediamine. The Bi-doped CQDs were then functionalized onto the liposomes by thin film hydration to prepare lipo/Bi-doped CQDs. More experimental details of the preparation process can be found in Supporting information. The morphology and size distribution of Bi-doped CQDs, liposomes, and lipo/Bi-doped CQDs were characterized by transmission electron microscopy (TEM) and atomic force microscopy (AFM). As shown by TEM and AFM in Figs. 1A, C, E, G, and Figs. S1 and S2A (Supporting information), the average particle sizes of Bi-doped CQDs, liposomes and lipo/Bi-doped CQDs are 2.7, 118.1, and 78.7 nm, respectively, and the heights are 2.8, 95, and 78 nm, respectively (Figs. 1D and H, and Fig. S2B in Supporting information), indicating that the shapes of the three materials are close to spherical. In addition, the lattice fringes in the high-resolution TEM (HRTEM) image in the inset of Fig. 1A show the lattice structure of the Bi-doped CQDs with a planar spacing of 0.21 nm, corresponding to the (100) plane of graphitic carbon [7]. The X-ray diffraction (XRD) patterns of the three materials are shown in Figs. 1B and F, and Fig. S3 (Supporting information), the diffraction peaks of the lipo/Bi-doped CQDs are composed of Bi-doped CQDs and liposomes, showing distinct peaks at about 19.3°, 21.4°, and 31.8°.

To further investigate the composition and properties of lipo/Bi-doped CQDs, we also analyzed the optical properties of Bi-doped CQDs, liposomes, and lipo/Bi-doped CQDs through ultraviolet–visible (UV–vis) absorption and fluorescence emission spectroscopy. Fig. 1I shows the UV–vis spectra of Bi-doped CQDs. The absorption peaks of the CQDs at 270 and 380 nm can be attributed to the C=C of the carbon core and the n-π^* transition of the surface groups, respectively [13]. The fluorescence spectra of Bi-doped CQDs also show excitation-dependent emission, which is consistent with the characteristics of most CQDs. As shown in Fig. 1J, the fluorescence emission peaks of the CQDs are slightly blue-shifted with the excitation wavelength increasing from 360 nm to 460 nm. This excitation-dependent emission characteristic may be related to the surface functional groups and the different surface gaps [17,20]. In addition, the absorption peak at 380 nm of the lipo/Bi-doped CQDs becomes weaker when the Bi-doped CQDs are bound to liposomes, and the optimal excitation wavelength is blue-shifted from 390 nm to 290 nm (Figs. 1I and K). These are the characteristics of CQDs encapsulated in liposomes [13,21]. We also analyzed the quantum yields (QYs) and time-resolved fluorescence attenuation curves of Bi-doped CQDs and lipo/Bi-doped CQDs solutions by steady transient fluorescence spectroscopy to observe the

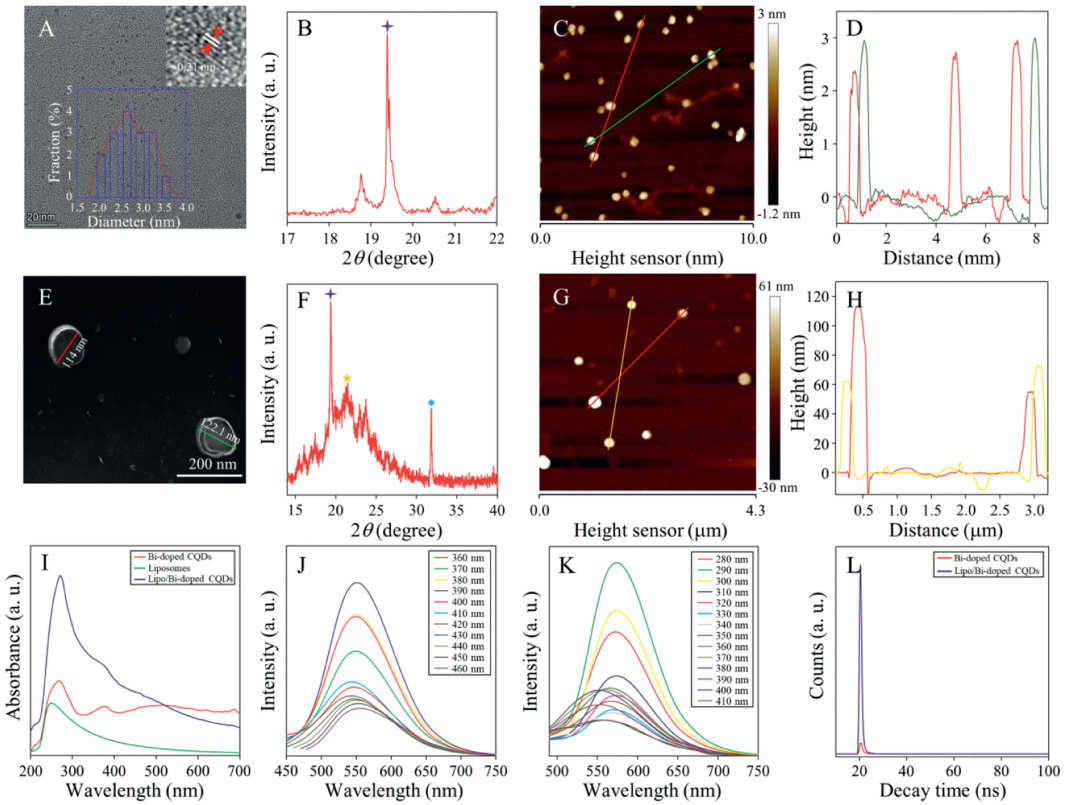

Fig. 1. TEM, XRD, AFM, and height distribution images of Bi-doped CQDs (A-D) and lipo/Bi-doped CQDs (E-H). Insets in A: Size distributions and HRTEM images of Bi-doped CQDs. (I) UV–vis absorption spectra of the three materials. The fluorescence spectra of Bi-doped CQDs (J) and lipo/Bi-doped CQDs (K) at different excitation wavelengths. (L) Time-resolved fluorescence attenuation curves of Bi-doped CQDs and lipo/Bi-doped CQDs.

effect of liposomes on the fluorescence properties of CQDs. The results showed that the fluorescence QY of the aqueous solution of Bi-doped CQDs increased 4 times, and the fluorescence lifetime decreased from 1.16 ns to 0.59 ns (Fig. 1L, Figs. S4, S5, and Table S1 in Supporting information). The decrease in fluorescence lifetime indicates that electrons were transferred during the transition, suggesting that the encapsulation of liposomes significantly improves the fluorescence characteristics of Bi-doped CQDs, which is of great significance in biomedicine [13,20,21]. Figs. S6 and S7 (Supporting information) show the photostability of the prepared Bi-doped CQDs and lipo/Bi-doped CQDs under different conditions, thus evaluating their practicability in diagnostics. As shown in Fig. S6, the fluorescence intensity of Bi-doped CQDs and lipo/Bi-doped CQDs showed almost no change after 60 min continuous UV light irradiation. Meanwhile, the fluorescence of the above two materials hardly changed in the constant spectroscopic tests with different salt solution concentrations (Fig. S7), indicating that Bi-doped CQDs and lipo/Bi-doped CQDs have good photostability and great potential for medical diagnosis and therapy (Scheme 1B).

The thermal stability of Bi-doped CQDs, liposomes, and lipo/Bi-doped CQDs was studied by thermogravimetric (TGA) analysis. As shown in Fig. 2A, the thermal stability of liposomes was higher than that of Bi-doped CQDs and lipo/Bi-doped CQDs. At 440 °C, the weight loss rates of Bi-doped CQDs and lipo/Bi-doped CQDs were 69.7% and 64.8%, respectively. The weighting ratio of the two materials reached 72% and 69.2% when the temperature reached 800 °C. For the liposomes, the mass rate at 440 °C was 44.8%, and then the weight loss rate at 800 °C was 46.3%, indicating that the content of Bi-doped CQDs encapsulated in the liposomes was 89.1 wt%, and the content of Bi elements was 0.71% [11]. We also further studied the valence bonding forms of functional groups on the surfaces of the three materials by Fourier transform infrared (FT-IR) and X-ray photoelectron (XPS) spectroscopy. As shown in Fig. 2B, liposomes and lipo/Bi-doped CQDs exhibit C-H stretching vibration in the range of 2900–2950 cm^{-1}, and C=O stretching vibration in the region of 1700–1800 cm^{-1} [22]. However, the absorption bands become less pronounced for the Bi-doped CQDs at the above two locations. Moreover, the characteristic O-H/N-H stretching vibrations of liposomes and lipo/Bi-doped CQDs were observed in the range of 3300–3400 cm^{-1} compared to Bi-doped CQDs. The absorption peaks of Bi-doped CQDs and lipo/Bi-doped CQDs in the field of 620–630 cm^{-1} can be attributed to -Bi-O tensile vibration [23,24], indicating the successful formation of composite nanomaterials between Bi-doped CQDs and liposomes. The XPS full spectra of Fig. 2C and Fig. S8 (Supporting information) show that the three materials are mainly composed of C, N, and O, and the percentages of different elements are listed in Table S2 (Supporting information). The high-resolution C 1s spectra (Figs. 2D and I, Fig. S9A in Supporting information) can be divided into parts of 284.3, 284.6, 285.0, 286.0, and 288.9 eV, belonging to the C=C, C-C, C-N, C-O, and C=O bonds respectively [20,25]. The high-resolution N 1s spectra have two distinct peaks at 401.9 and 402.2 eV, which are attributed to the pyrrole N and N-H bonds (Figs. 2E and J, Fig. S9B in Supporting information). The high-resolution O 1s spectra of lipo/Bi-doped CQDs (Fig. 2F) show three peaks at 530.5, 532.2, and 533.3 eV, corresponding to Bi-O, P-O, and C=O bonds, respectively, compared to the Bi-doped CQDs (Fig. 2K) and liposomes (Fig. S9C in Supporting information) [25,26]. In addition, the high-resolution Bi 4f spectra of Bi-doped CQDs (Fig. 2L) and lipo/Bi-doped CQDs (Fig. 2G) can be divided into 158.84 and 164.44 eV, which are associated with Bi $4f_{7/2}$ and Bi $4f_{5/2}$ structures, respectively [23,24,26]. The high-resolution P 2p of lipo/Bi-doped CQDs and liposomes in Fig. 2H and Fig. S9D (Supporting information) show two distinct peaks at 132.9 and 133.54 eV, mainly in the form of P-C and

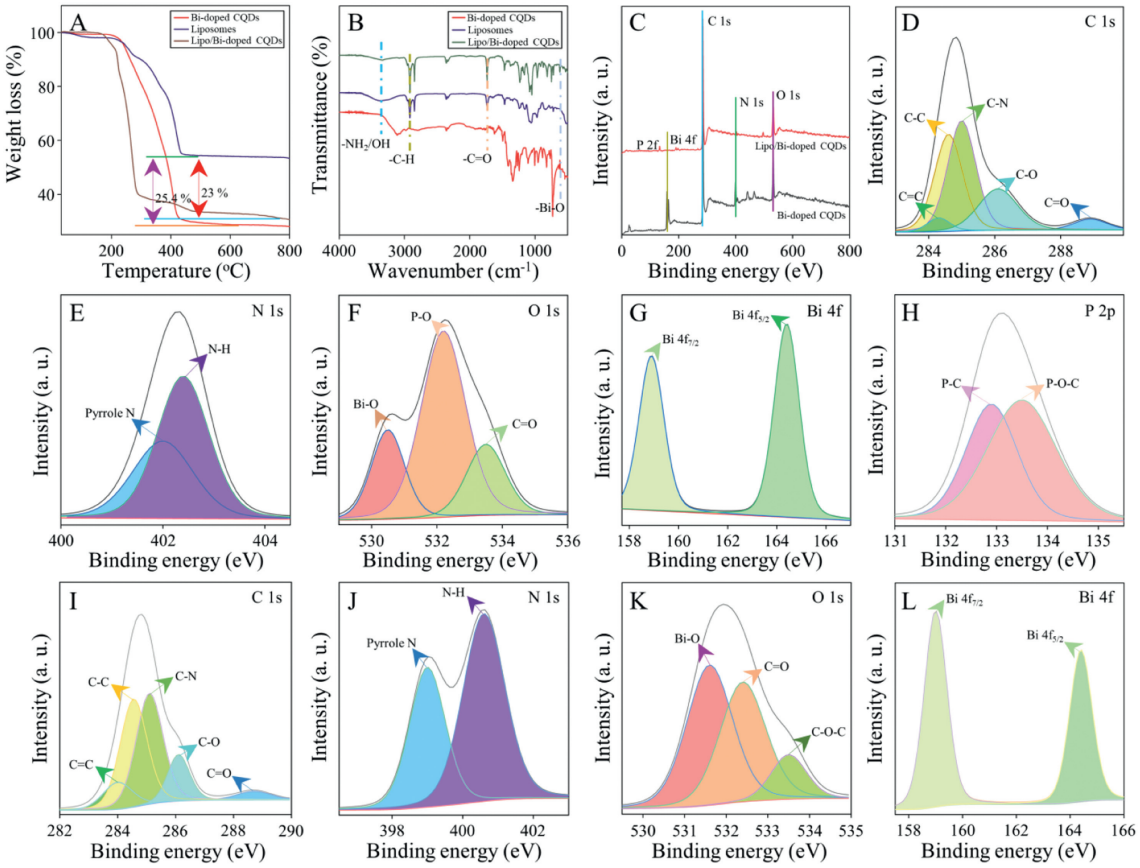

Fig. 2. TGA (A) and FT-IR (B) analysis of Bi-doped CQDs, liposomes, and lipo/Bi-doped CQDs. XPS survey spectrum (C) of lipo/Bi-doped CQDs and Bi-doped CQDs. High-resolution XPS of C 1s (D), N 1s (E), O 1s (F), Bi 4f (G), P 2p (H) and C 1s (I), N 1s (J), O 1s (K), Bi 4f (L) spectra of lipo/Bi-doped CQDs and Bi-doped CQDs.

P-C-P bonds [26]. Overall, the functional groups observed in the XPS spectra are consistent with the FT-IR spectra, indicating that the lipo/Bi-doped CQDs are composed of Bi-doped CQDs and liposomes, and the nitrogen and oxygen functional groups contained on the surface confer excellent water solubility of the material.

The optical properties and structural analysis of Bi-doped CQDs and lipo/Bi-doped CQDs showed that the materials have good photostability and water solubility and have promising applications prospects in biomedicine (Figs. 1 and 2, Figs. S6 and S7) [20,22]. First, we chose CT26 cells as a cell model to evaluate the cytotoxicity of Bi-doped CQDs and lipo/Bi-doped CQDs (Fig. S10 in Supporting information). Secondly, different concentrations of Bi-doped CQDs and lipo/Bi-doped CQDs were co-cultured with CT26 cells for 24 h. Finally, the experimental results showed that the half-maximum inhibitory concentration of Bi-doped CQDs and lipo/Bi-doped CQDs on CT26 cells was about 0.38 mg/mL, indicating that liposomes have good biocompatibility and low biotoxicity [2,27].

To investigate the imaging ability of Bi-doped CQDs and lipo/Bi-doped CQDs in tumor cells, we evaluated the fluorescence imaging of CT26 cells with two materials by inverted laser fluorescence microscopy. Fig. S11 (Supporting information) shows typical images of CT26 cells incubated with 4,6-diamidino-2-pheny-lindole (DAPI), Bi-doped CQDs, and lipo/Bi-doped CQDs. The Bi-doped CQDs and lipo/Bi-doped CQDs groups showed bright blue fluorescence due to the staining of the nucleus by DAPI, while the red fluorescence of CT26 cells is from Bi-doped CQDs. In addition, the merged images showed the intracellular and extracellular distribution of Bi-doped CQDs and lipo/Bi-doped CQDs. Due to the passive targeting of liposomes, lipo/Bi-doped CQDs showed outstanding intracellular uptake and intense fluorescence imaging effects [28]. This suggests that liposomes as a nanocarrier system for drugs can help to improve the cellular uptake of Bi-doped CQDs. Furthermore, to analyze the drug release rate of liposomes at different pH values, we measured the fluorescence intensity changes of Bi-doped CQDs and lipo/Bi-doped CQDs at different pH values. As shown in Fig. 3A-a1, the fluorescence intensity of Bi-doped CQDs at 550 nm gradually increased when the pH value was varied from 3 to 9, and showed a decreasing trend in CQDs solution with strong acidic (pH 1) or higher pH values (pH 11 or 13). Conversely, the fluorescence intensity of lipo/Bi-doped CQDs was strongest at pH 5 in successive pH values from 3 to 9 (Fig. 3B-b1). The change in fluorescence intensity of lipo/Bi-doped CQDs may be related to the degradation rate of liposomes. Therefore, we also labeled CT26 cells with Bi-doped CQDs and lipo/Bi-doped CQDs at pH 3, 5, and 7 for fluorescence imaging under an inverted laser fluorescence microscope. The fluorescence of Bi-doped CQDs in CT26 cells gradually increased when the pH was varied from 3 to 7 (Fig. 3A-a2). In contrast, the fluorescence color of lipo/Bi-doped CQDs in CT26 cells showed an increase followed by a decrease (Fig. 3B-b2), which was consistent with the fluorescence spectra of the materials at different pH values, indicating that liposomes have the best drug release rate in a weak acid environment [29,30].

Inspired by the intracellular results, we further investigated the biodistribution and tumor-targeting ability of Bi-doped CQDs and lipo/Bi-doped CQDs in tumor-bearing mice. Animal experiments were conducted following the guidelines for the use and care of animals issued by the Animal Ethics Committee of Huazhong University of Science and Technology Union Shenzhen Hospital. CT26 tumor-bearing BALB/c mice were used as models, Bi-doped CQDs and lipo/Bi-doped CQDs were injected into the mice by intravenous

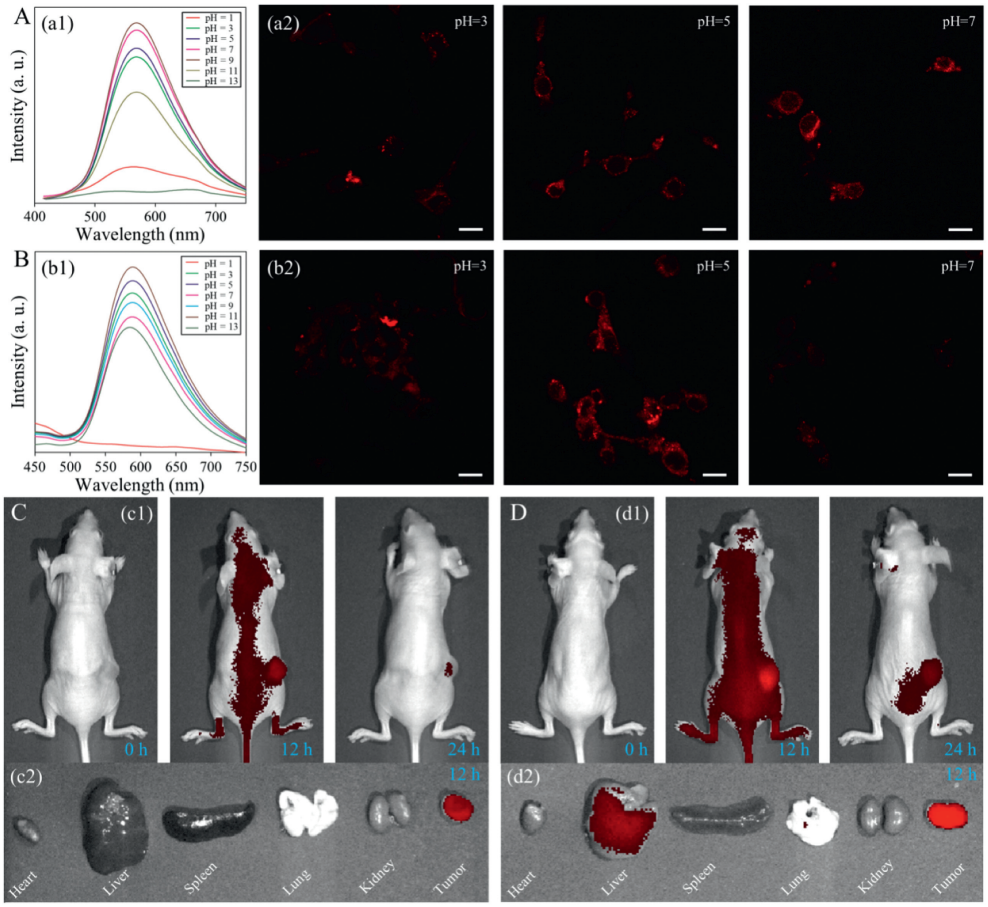

Fig. 3. (A) Fluorescence spectra (a1) and *in vitro* fluorescence (a2) imaging of Bi-doped CQDs at different pH values. (B) Fluorescence spectra (b1) and *in vitro* fluorescence (b2) imaging of lipo/Bi-doped CQDs at different pH values. (C) *In vivo* fluorescence (c1) and major organ (c2) imaging of Bi-doped CQDs at different times and 12 h. (D) *In vivo* fluorescence (d1) and major organ (d2) imaging of lipo/Bi-doped CQDs at different times and 12 h. Scale bar: 30 μm.

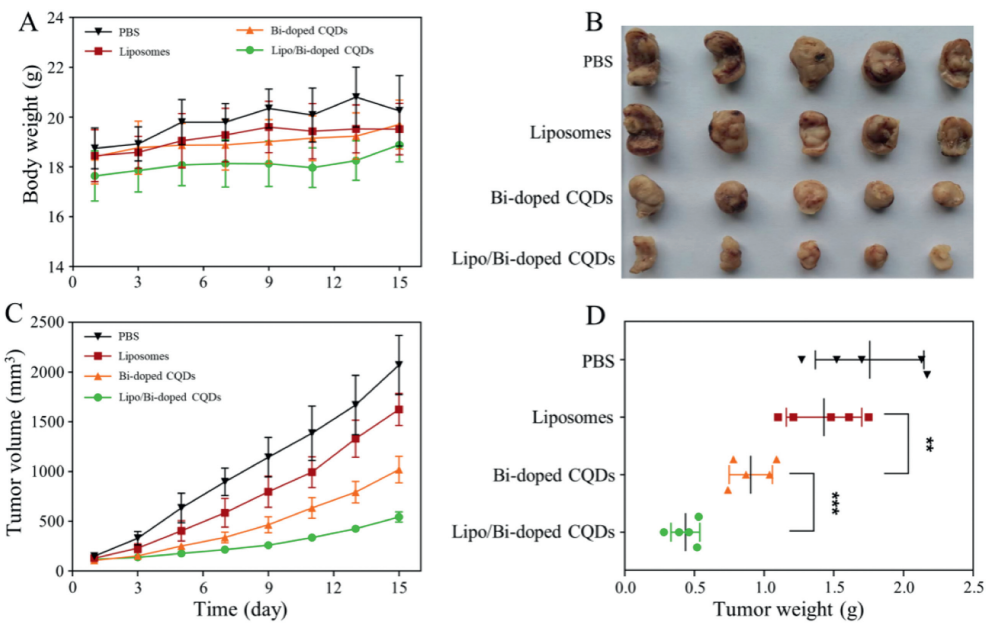

Fig. 4. (A) Body weight of mice after different treatments ($n = 5$). (B) Tumor pictures of mice after 15 days. (C) Tumor volume ratio of mice in different treatment processes ($n = 5$). (D) Tumor mass of mice after different treatments (mean ± standard deviation (SD), $^{**}P < 0.01$, $^{***}P < 0.001$).

injection, respectively. As shown in Figs. 3C and D, 12 h after injection, the lipo/Bi-doped CQDs showed a noticeable red fluorescence at the tumor site and a faint fluorescence in the liver. In contrast, the imaging ability of Bi-doped CQDs was relatively weak, suggesting that liposomes as nanocarriers contributed to the accumulation of Bi-doped CQDs in the tumors. In addition, we evaluated the relationship between tumor growth changes and the anti-cancer efficiency of lipo/Bi-doped CQDs. Mice in each group were injected with samples intravenously at different time points on days 1, 3, and 5, and body weight and tumor volume were monitored every 2 days. As shown in Fig. 4A, the body weight of mice was maintained between 17.8 g and 20.5 g, indicating that the effect of samples on the body weight of mice was negligible. After 15 days of treatment, lipo/Bi-doped CQDs showed good inhibition of tumor growth (Fig. 4B). In contrast, the PBS group showed an approximately 20-fold increase in tumor volume and an approximately 4-fold increase in tumor mass (Figs. 4C and D). These results suggest that lipo/Bi-doped CQDs have better therapeutic effects.

Encouraged by the efficacy of the tumor treatment, we further validated the *in vivo* cytotoxicity of the material and examined slices of the major organs collected at the end of the treatment. The slices were stained with hematoxylin and eosin (H&E), as shown in Fig. S12 (Supporting information). No significant abnormalities were observed in the major organs of the four groups of mice, indicating that the good biocompatibility of the lipo/Bi-doped CQDs.

In summary, we have demonstrated the therapeutic potential of a theranostic agent, lipo/Bi-doped CQDs, with bright internal emission. The lipo/Bi-doped CQDs can be visualized by fluorescence imaging, and the cellular uptake process and drug release rate of liposomes at different pH values can be detected through bright and stable fluorescence signals, overcoming the defects of conventional dye-modified liposomes. Meanwhile, due to the passive targeting and drug release properties of liposomes, the drug content of Bi-doped CQDs in tumors is increased, and the visual therapeutic effect of tumors is improved. Lipo/Bi-doped CQDs showed good tumor treatment and imaging effects *in vivo*, which could be verified by the adequate visualization time of cancer. Therefore, the functionalization of Bi-doped CQDs in liposomes is a feasible design for a diagnostic and therapeutic agent with inherent fluorescence imaging guidance and efficient targeting capabilities.

Declaration of competing interest

The authors declare that they have no known competing financial interests or personal relationships that could have appeared to influence the work reported in this paper.

Acknowledgments

The research is funded by Beijing Natural Science Foundation (Nos. L222109, 3222018), Military Health Care Project (No. 22BJZ22), Science Foundation of China University of Petroleum (Nos. 2462019QNXZ02, 2462019BJRC007), National Natural Science Foundation of China (Nos. 52211530034, 82273236), Guangdong Provincial Basic and Applied Basic Research Foundation (Nos. 2022A151522004, 2022A1515220042), Science and Technology Innovation Commission of Shenzhen (Nos. JSGG20210802153410031, JCYJ20220530141609021), Science and Technology Plan of Shenzhen Nanshan District (No. NS016), Discipline Leader Foundation of Huazhong University of Science and Technology Union Shenzhen Hospital (No. YN2021002), and Crosswise Project of Daan Gene (No. HXKY2022002).

Supplementary materials

Supplementary material associated with this article can be found, in the online version, at doi:10.1016/j.cclet.2023.108689.

References

[1] D. Bouzas-Ramos, J.C. Canga, J.C. Mayo, et al., Adv. Funct. Mater. 29 (2019) 1903884.
[2] M. Hashemi, J. Mohammadi, M. Omidi, et al., Mat. Sci. Eng. C 103 (2019) 109860.
[3] C. Hang, T.J. Liu, Z.Q. Su, et al., Nanoscale Horiz. 3 (2018) 74–89.
[4] B. Wang, G. Waterhouse, S. Lu, Trends Chem. 5 (2023) 76–87.
[5] A. Topete, M. Alatorre-Meda, P. Iglesias, et al., ACS Nano 8 (2014) 2725–2738.
[6] S.Y. Lee, M.J. Shieh, ACS Appl. Mater. Interfaces 12 (2020) 4254–4264.
[7] J. Zhong, X. Chen, L. He, et al., Chin. Chem. Lett. 31 (2020) 769–773.
[8] H. Zhao, Y. Chao, J.J. Liu, et al., Theranostics 6 (2016) 1833–1843.
[9] C. Liang, S. Diao, C. Wang, et al., Adv. Mater. 26 (2014) 5646–5652.
[10] X. Yang, G. Li, L. Ai, et al., Chin. Chem. Lett. 33 (2022) 613–625.
[11] Y. Su, S. Liu, Y. Guan, et al., Biomaterials 255 (2020) 120110.
[12] F.Y. Du, L.R. Zhang, L. Zhang, et al., Biomaterials 121 (2017) 109–120.
[13] C. Guan, Y.Y. Zhao, Y.T. Hou, et al., Talanta 182 (2018) 314–323.
[14] X.L. Cai, D. Mao, C. Wang, et al., Angew. Chem. Int. Ed. 57 (2018) 16396–16400.
[15] G. Aizik, N. Waiskopf, M. Agbaria, et al., Nano Lett. 19 (9) (2019) 5844–5852.
[16] D.N. Williams, P. Sunipa, R.P. Brown, et al., ACS Appl. Nano Mater. 1 (2018) 4788–4800.
[17] T. Feng, X.Z. Ai, G.H. An, et al., ACS Nano 10 (2016) 4410–4420.
[18] T. Malina, K. Poláková, J. Skopalík, et al., Carbon 152 (2019) 434–443.
[19] P.W. Gong, S. Lu, F. Wang, et al., Chem. Eng. J. 356 (2019) 994–1002.
[20] B. Wang, Z. Wei, S. Lu, et al., Light Sci. Appl. 11 (2022) 172.
[21] W. Ren, S.Q. Chen, Y.Y. Liao, et al., Colloids Surf. B: Biointerfaces 175 (2018) 384–392.
[22] P.D. Zhu, X.L. Zhao, Y.Q. Zhang, et al., Front Bioeng. Biotechnol. 10 (2022) 964814.
[23] P.J. Weng, Q. Cai, H.D. Wu, et al., J. Mater. Sci. 57 (2022) 19771993.
[24] F.T. Yi, J.Q. Ma, C.W. Lin, et al., J. Alloy. Compd. 821 (2019) 153557.
[25] P. Zhu, W. Li, L.L. Cai, et al., Chin. Chem. Lett. 34 (2023) 108239.
[26] S.J. Zhang, Y.M. Zhang, Z.Y. Zhang, et al., Adv. Energy Mater. 12 (2022) 2103888.
[27] Z.K. Chen, Y.N. Tu, D. Zhang, et al., Biomater. Sci. 8 (2020) 4299–4307.
[28] S.A. Moosavian, A. Sahebkar, Cancer Lett. 448 (2019) 144–154.
[29] M. Hashemi, M. Omidi, B. Muralidharan, et al., Acta Biomater. 65 (2018) 376–392.
[30] M. Barattin, A. Mattarei, A. Balasso, et al., ACS Appl. Mater. Interfaces 10 (2018) 17646–17661.